

4/16/91
E5975

NASA Technical Memorandum 103738

Performance of a High-Work, Low-Aspect-Ratio Turbine Stator Tested With a Realistic Inlet Radial Temperature Gradient

Roy G. Stabe and John R. Schwab
Lewis Research Center
Cleveland, Ohio

March 1991

NASA

PERFORMANCE OF A HIGH-WORK, LOW-ASPECT-RATIO TURBINE STATOR TESTED
WITH A REALISTIC INLET RADIAL TEMPERATURE GRADIENT

Roy G. Stabe and John R. Schwab
National Aeronautics and Space Administration
Lewis Research Center
Cleveland, Ohio 44135

SUMMARY

A 0.767-scale model of a turbine stator designed for the core of a high-bypass-ratio aircraft engine was tested with uniform inlet conditions and with an inlet radial temperature profile simulating engine conditions. The principal measurements were radial and circumferential surveys of stator-exit total temperature, total pressure, and flow angle. The stator-exit flow field was also computed by using a three-dimensional Navier-Stokes solver. Other than temperature, there were no apparent differences in performance due to the inlet condition. The computed results compared quite well with the experimental results.

INTRODUCTION

This report presents the results of an experimental investigation of the three-dimensional flow field at the exit of a turbine stator. The test stator was that for a research turbine designed as a part of Lewis' Energy Efficient Engine Program. The turbine was designed to be similar to the first stage of the turbines used in modern high-bypass-ratio aircraft engines. The stator had a 75° exit flow angle to accommodate the high-work, low-flow characteristics of these turbines. The turbine design information and its overall performance are reported in reference 1.

The stator was tested in the annular cascade rig in the Warm Core Turbine Facility, which is described in reference 2. The principal measurements were radial and circumferential surveys of total temperature, total pressure, and flow angle at the stator exit. These measurements were made both with a uniform inlet temperature and with a radial inlet temperature profile similar to a combustor-exit temperature profile. The data presented include contour plots of the survey measurements over one vane space and also circumferentially averaged values showing the radial variations of several performance parameters.

The flow field was also computed by using a three-dimensional Navier-Stokes solver specifically intended for turbomachinery applications (ref. 3). The experimental data were compared with computed results.

SYMBOLS

M	Mach number
m	equivalent mass flow, kg/sec cm ²
P	pressure, kPa

T temperature, K
V velocity, m/sec
 α flow angle, deg
 θ circumferential position, deg

Subscripts:

0, 1, 2, 3 instrument stations (fig. 3)
cr flow conditions at Mach 1
M after-mix value

Superscripts:

' total state conditions
- inlet average value

APPARATUS AND PROCEDURE

Test Facility

The Warm Core Turbine Facility is shown in figure 1 and the test section in figure 2. The facility is described in some detail in reference 2. Air was supplied to the cascade by the laboratory 40-psig combustion air system. An automatic control valve maintained the inlet pressure at 207 kPa (30 psia) for these tests. After flowing through the stator the air was throttled to the altitude exhaust system through a manually controlled exhaust valve that controlled the stator pressure ratio. The primary air was heated with a natural gas combustor as shown in figure 1. The airflow and fuel flow were measured with calibrated venturi flowmeters.

The CERTS inlet section used in the turbine test (ref. 1) was also used in the annular cascade. CERTS is an acronym for "combustion exit radial temperature simulator." A schematic diagram of this inlet section is shown in figure 3. The stator-inlet radial temperature profile was adjusted by individually controlling and measuring the airflow through each of the four slots shown in figure 3.

Stator Design

The test stator was the same stator used in the turbine tests. It is shown in figure 4. The principal design criteria were smooth surface velocity or pressure distribution, with minimal diffusion, reasonable Mach number levels and vane heights, and a small number of vanes. The MERIDL and TSONIC programs (refs. 4 and 5) were used to determine the vane surface velocities and pressures. The pressure distribution P/P_1' is shown in figure 5. The vanes were a constant-angle, constant-section design, and the stator endwalls were cylindrical to simplify fabrication. The stator dimensions and selected design parameters are listed in tables I and II. More complete design information can be found in reference 1.

Instrumentation

The location of the instrument stations is shown in figure 6. At station 0 (fig. 3) the total temperature upstream of the CERTS slots was measured with 20 thermocouples, 5 on each of the 4 inlet struts. The average temperature at the stator inlet was calculated from measured flow rates and the temperatures of the primary and CERTS flows.

Inlet static pressure was measured with five static taps each on the inner and outer wall at station 1. Inlet average total pressure was calculated from temperature, static pressure, and flow measurements. Stator-exit static pressure was measured at station 2 with 17 static taps each on the hub and tip walls. These taps were closely spaced across one vane exit passage. Three stator vanes were instrumented with 10 static taps each. These were located at the hub, mean radius, and tip sections, respectively. The axial location of these taps is indicated in figure 5.

Inlet surveys of total temperature and pressure were made at the stator inlet, (station 1). A small, shielded thermocouple probe was used for a radial survey of the inlet total temperature at station 1. The inlet total pressure radial survey probe was electrically insulated from the cascade casing so that probe contact with the hub wall could be detected. The probe tip was a 0.5-mm tube flattened to 0.35 mm.

The radial and circumferential actuators used for the surveys at the stator exit are shown in figure 7. Two types of probe were used for these surveys. The sting probe shown measures total pressure and temperature at two radial locations simultaneously, both 1.6 cm from the stator trailing edge (station 2). The other probe was a standard cobra type that measures total pressure, temperature, and flow angle. It was used for the surveys taken 3.0 cm behind the stator trailing edge (station 3).

Experimental Procedure

The cascade was operated at a constant inlet pressure of 207 kPa (30 psia) and at a stator-inlet total to stator-exit static pressure ratio of 1.72. This is the pressure ratio at which the stator operated in the turbine test. The design pressure ratio was 1.56. Data were taken with a uniform inlet temperature of 422 K (300 °F) and also with the CERTS air turned on to provide a radial temperature gradient. The average inlet temperature in the latter case was 672 K (750 °F).

Stator-exit surveys were made 3.0 cm axially downstream of the stator trailing edge with the self-aligning cobra probe and 1.6 cm axially downstream with the sting probe. The probes were moved circumferentially at constant radius. Data were recorded at 25 locations spanning one vane space. This process was repeated at 15 radial positions. The results of radial and circumferential surveys were used to construct contour plots of stator-exit temperature, total pressure loss, Mach number, flow angle, and mass flow. A momentum mixing procedure described in reference 6 was used to obtain circumferentially averaged values of these parameters. These values are used to show the variation of each parameter as a function of vane height. The same procedure was used to circumferentially average the computed results.

Computational Procedure

A finite-volume Navier-Stokes code (ref. 3) was used for the flow prediction. The basic algorithm time-marches the unsteady three-dimensional governing equations with a two-step explicit and one-step implicit scheme. The Baldwin-Lomax mixing-length turbulence was used with a constant turbulent Prandtl number of 0.9. Combined second-derivative and fourth-derivative artificial viscosity was used to filter odd-even decoupling and thus to damp transients in the solution. The overall smoothing factors in the radial and circumferential directions were reduced to 10 percent of the axial smoothing factors in order to minimize smoothing of the flow profiles in the radial and circumferential planes.

The computational grid consisted of 60 points in the axial direction and 21 points in the radial and circumferential directions. The upstream boundary was placed 3.0 cm upstream of the vane leading edge to match experimental measurement station 1, and the downstream boundary was placed 3.0 cm downstream of the vane trailing edge to match experimental measurement station 3. The grid was axially packed near the leading and trailing edges as well as radially and circumferentially packed near the endwall and vane surfaces. The total pressure, total temperature, and flow angle profiles at the upstream boundary and the static pressure at the exit at the downstream boundary were fixed to match the experimental data. Adiabatic no-slip conditions were specified at the vane and endwall surfaces along with a zero normal pressure gradient. The wall shear stress was computed with a logarithmic skin friction law.

This case required 3584 sec of Cray X/MP time for 2000 iterations on the 21 by 60 by 21 grid, resulting in an overall speed of 67.7 μ sec per iteration per grid point. The multigrid acceleration scheme mentioned in reference 3 was not available in the version of the code used for this case. Convergence was taken to be when the overall mass flow error stabilized below 0.5 percent and the other flow parameters reached an apparent stable value.

RESULTS AND DISCUSSION

The results presented include data from the radial surveys of inlet total pressure and temperature, contour plots of several parameters derived from the radial and circumferential surveys at the stator exit, and the radial variation of these parameters determined from circumferentially averaged data. Computed results for a similar set of parameters at the stator exit are also shown.

Inlet Conditions

The stator-inlet radial temperature profile generated by the CERTS inlet secondary air is shown in figure 8. The uniform inlet temperature was 422 K, the same as that used in the turbine tests (ref. 1).

The stator-inlet radial total pressure loss profile is shown in figure 9 for both inlet temperature conditions. The total pressure loss was small but extended far into the inlet passage. This was probably due to the long (20 cm) CERTS inlet section. The use of the CERTS secondary air increased the pressure loss at the hub wall and essentially eliminated the normal free-stream condition of no loss.

Vane Surface Static Pressure

The measured vane static pressure distribution is shown in figure 5 along with the design values and the results of the three-dimensional viscous calculation. Pressures rather than surface velocities are shown because the vane surface static pressures were measured directly and did not require any assumptions as to the loss distribution in the vane passage.

The measured and computed static pressures on the pressure surface agreed closely with the design values. On the suction surface the computed values also agreed fairly well with the measured pressures. However, both measured and computed static pressure were lower (higher loading) than design over the last part of the vane suction surface. This was particularly evident at the tip section and occurred because the stator was operated at a higher-than-design pressure ratio. The constant static pressure measured over the last 15 percent of axial chord on the suction surface at the hub section indicated that flow separation probably occurred in this region. Flow separation would result in larger loss at the hub section.

Stator-Exit Surveys

Contour plots constructed from the data acquired in the stator-exit surveys are shown in figures 10 to 14. These data are shown for both inlet conditions at both locations, 1.6 cm and 3.0 cm axially downstream of the stator trailing edge, as appropriate. The 1.6 cm location corresponds to the rotor leading edge. The computed results are shown for the 3.0 cm location and for an inlet temperature gradient only.

The contour plots cover one vane space, 13.85° from the hub to the tip radius. The surveys were made so that the wake was centered in this region at the mean radius. The results were plotted on a regular segment. The computed results covered the same region, but these plots show how the flow field was skewed in passing through the stator.

Total temperature data are shown in figure 10 as the ratio of the local total temperature to the upstream averaged total temperature. In general, the experimental data for station 2 (fig. 10(a)) and station 3 (fig. 10(b)) show that the hotter regions were near the midspan but the cooler regions remained near the hub and tip endwalls. The station 2 data (fig. 10(a)) show an isolated temperature region near the hub endwall that does not appear in the station 3 data (fig. 10(b)). The computed results in figure 10(c) show the same general trend of a hotter midspan region with cooler endwall regions, but the overall midspan temperatures were higher than the experimental data in figures 10(a) and (b). An isolated hot spot occurred near the hub endwall that distorted the more regular cooler-to-hotter-to-cooler spanwise trend.

Total pressure loss data are shown in figure 11 as the ratio of the local total pressure loss to the upstream averaged total pressure. Figures 11(a) and (b) show the experimental data taken with the inlet temperature profile at stations 2 and 3, respectively; figures 11(c) and (d) show similar data taken without the inlet temperature profile. These data are all very similar, with clearly defined skewed wakes and high loss regions near the endwalls; the hub endwall had substantially higher losses than the tip endwall. The addition of the inlet temperature profile did not appear to have much effect on the experimental total pressure loss data. The

computed results with the inlet temperature profile in figure 11(e) show the same overall features as the experimental data (figs. 11(a) to (d)), but a broader wake region with higher losses is evident along with more extensive losses from the hub endwall to the midspan region.

Experimental flow angle data taken at station 3 are shown in figures 12(a) and (b) with and without the inlet temperature profile, respectively. Both figures show similar high turning near the tip endwall with a return to more moderate turning near the midspan and hub endwall regions. The overall turning appears to be less than the design value of 75° . The computed results with the inlet temperature profile in figure 12(c) appear to be more circumferentially uniform than the experimental data, but the flow angle sharply diminished to less than 70° between approximately 90 and 70 percent of the span. The flow angle gradually returned to the design value of 75° through the midspan region before increasing near the hub endwall.

The experimental Mach number data with the inlet temperature profile at stations 2 and 3 are shown in figures 13(a) and (b), respectively; figures 13(c) and (d) show similar data without the inlet temperature profile. Little difference is discernible between the data with and without the profile; some additional diffusion is evident for the data at station 3 compared with those at station 2. A skewed wake appears in each figure along with a general trend of higher velocities toward the hub region and lower velocities toward the tip region. The hub boundary layer was generally thicker than the tip boundary layer. The computed results with the inlet temperature profile in figure 13(e) show a more defined skewed wake with lower midspan velocities. The high velocities near the hub found in the experimental data did not appear in the computed results. The hub and tip endwall boundary layers appeared to be approximately equal in thickness.

Equivalent mass flow data in kilograms per second per square centimeter are shown in figures 14(a) and (b) with and without the inlet temperature profile, respectively. These plots are very similar and show a general trend of slowly varying mass flow in the midspan with rapidly diminishing mass flow in the hub and tip endwall boundary layers. The computed results with the inlet temperature profile are shown in figure 14(c). The general trend in these data is a sharp peak in the mass flow from approximately 70 to 90 percent of the span and a gradual decrease toward the hub region. The sharp peak extends across the entire blade passage and is consistent with the computed underturning shown previously in figure 12(c). Rapidly diminishing mass flow was again evident in both the hub and tip endwall boundary layers.

Radial Variation of Circumferentially Averaged Data

The data from the radial and circumferential surveys and from the computed results were processed by using a momentum mixing procedure (ref. 6) that calculates after-mix values at a hypothetical downstream location (station 3M) where the flow conditions were assumed to be circumferentially uniform. This procedure calculates circumferentially averaged values of pressure, temperature, velocity, flow angle, and mass flow. The results were used to construct the radial variations of these parameters shown in figures 15 to 20.

The radial variation of the stator-exit total temperature ratio T'_{3M}/T'_1 is shown in figure 15. The inlet temperature profile is also shown in this figure for

comparison. The test data show that some mixing occurred in the stator passage. A small amount of mixing also occurred between the two survey planes. The computed exit temperature profile over most of the vane height is similar to the inlet temperature profile but does show some mixing near the stator hub.

The radial variation of stator-exit total pressure is shown as a pressure loss coefficient $(\bar{P}'_1 - \bar{P}'_{3M})/\bar{P}'_1$ in figure 16. There was very little difference between the four variations of inlet condition and exit survey location except for a small increase in loss at the tip section between the two survey planes. The shape of the loss curve is similar to that for the inlet loss, but the loss is much larger, particularly at the hub section where significant loss extends up to 30 percent of the vane height. The loss at the mean section was 2 percent of the inlet total pressure, which was the design value. The overall loss was 5.5 percent of the inlet total pressure. The computed pressure loss also showed large endwall losses and these agreed very well with the experimental data. The agreement was not quite so good in the midspan region, where the computed loss was up to 5 percentage points larger than the experimental loss. The large endwall losses were a consequence of the thick boundary layer in the long CERTS inlet and also of flow separation at the vane hub suction surface.

The radial variation of stator-exit flow angle is shown in figure 17. The flow angle was slightly larger in the midspan region for the uniform inlet case. Otherwise, there was no difference in flow angle between the two inlet conditions. The flow angle increased to about 79° from axial at the tip section for both inlet conditions. The average angle was 73.8° with an inlet radial temperature profile and 74.0° with a uniform inlet temperature. The design angle was 75° , constant from hub to tip. The computed flow angle curve is similar in shape to the experimental data, differing by only 2° to 3° . Both curves have a minimum at 80 percent of span and increase rapidly at the tip section.

The radial variation of the stator-exit critical velocity ratio $(V/V_{cr})_{3M}$ is shown in figure 18. This curve reflects the pressure loss data discussed previously. The velocity was higher than the design values in the midspan region because of the higher-than-design stator operating pressure ratio. The computed velocity distribution is flatter and lower than the experimental results, but the agreement is good at the hub and tip sections. Both curves show a small peak at about 25 percent span.

The radial variation of equivalent mass flow per unit vane height is shown in figure 19. The mass flow deficits at the hub and tip sections were due to the large pressure losses in these regions and also to the large flow angle at the tip section. These data agreed very well with the measured flow, which averaged 0.034 kilogram per second per centimeter of vane height. There was no apparent difference due to the inlet condition. The computed mass flow curve is slightly lower at the hub region than the experimental results and has a more pronounced peak at about 80 percent span. However, the agreement between computed and experimental values is generally fairly good.

The radial variation of rotor inlet relative flow angle was calculated from the flow angle and velocity data. The results are shown in figure 20 along with the design angle. The rotor for the turbine of reference 1 was designed to operate with about 5° of positive incidence, the difference between the relative flow angle and the blade angle. However, the rotor was apparently operating with larger-than-design positive incidence over most of the blade height. From the hub section to 15 percent

of blade height, the incidence angles were negative. The increment in loss due to these incidence angles amounts to 0.5 percent in the rotor energy loss coefficient (ref. 7). The very large negative incidence angles at the hub section, however, imposed an additional penalty on turbine performance as they caused a negative loading on the rotor blade leading edge. The computed rotor inlet relative flow angle was very close to the design intent. In this case the smaller incidence angles were due to the higher computed loss and attendant lower velocity in the midspan region.

SUMMARY OF RESULTS

A turbine stator designed for the core of a high-bypass-ratio aircraft engine was tested with a radial inlet temperature profile and with uniform inlet conditions. The principal measurements were radial and circumferential surveys of stator-exit total temperature, total pressure, and flow angle. The stator-exit flow field was also computed by using a three-dimensional Navier-Stokes code. The following results were obtained:

1. Other than exit temperature gradient, using an inlet temperature profile caused no apparent difference in stator aerodynamic performance compared with uniform inlet conditions.

2. Large total pressure losses were measured at the stator hub and tip sections. These were attributed both to boundary layer growth in the long special inlet section used to generate the radial temperature profile and to flow separation at the vane hub suction surface.

3. The three-dimensional viscous computed results generally compared quite well with the experimental data.

REFERENCES

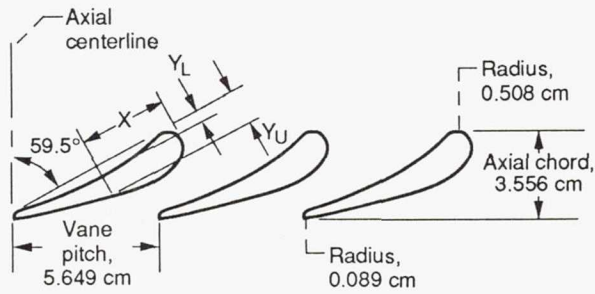
1. Stabe, R.G.; Whitney, W.J.; and Moffitt, T.P.: Performance of a High-Work Low Aspect Ratio Turbine Tested With a Realistic Inlet Radial Temperature Profile. AIAA Paper 84-1161, June 1984. (Also NASA TM-83655.)
2. Whitney, W.J.; Stabe, R.G.; and Moffitt, T.P.: Description of the Warm Core Turbine Facility Recently Installed at NASA Lewis Research Center. NASA TM-81562, 1980.
3. Dawes, W.N.: Development of a 3D Navier-Stokes Solver for Application to All Types of Turbomachinery. ASME Paper 88-GT-70, June 1988.
4. Katsanis, T.; and McNally, W.D.; Revised FORTRAN Program for Calculating Velocities and Streamlines on the Hub-Shroud Midchannel Stream Surface of an Axial-, Radial-, or Mixed-Flow Turbomachine or Annular Duct - I, User's Manual. NASA TN D-8430, 1977.
5. Katsanis, T.: FORTRAN Program for Calculating Transonic Velocities on a Blade-to-Blade Stream Surface of a Turbomachine. NASA TN D-5427, 1969.

6. Goldman, L.J.; and McLallen, K.L.: Cold-Air Annular Cascade Investigation of Aerodynamic Performance of Cooled Turbine Vanes - I, Facility Description and Base (Solid) Vane Performance. NASA TM X-3006, 1974.
7. Stabe, R.G., and Kline, J.F.: Incidence Loss for a Core Turbine Rotor Blade in a Two-Dimensional Cascade. NASA TM X-3047, 1974.

TABLE I. - TURBINE STATOR GEOMETRY

Mean diameter, cm	46.744
Mean vane pitch, s_m , cm	5.648
Vane height, b , cm	3.564
Axial chord, c_x , cm	3.556
Axial solidity, c_x/s_m	0.630
Aspect ratio, b/c_x	1.000
Number of vanes	26
Leading-edge radius, cm	0.508
Trailing-edge radius, cm	0.089
Zweifel coefficient	0.794
Exit flow angle, deg from axial	75.00

TABLE II.- STATOR VANE COORDINATES



X	Y_L	Y_U	X	Y_L	Y_U
0	0.509	0.509	3.800	0.587	1.133
.200	.105	1.064	4.000	.568	1.084
.400	.012	1.221	4.200	.546	1.035
.600	.008	1.319	4.400	.520	.983
.800	.089	1.385	4.600	.492	.930
1.000	.193	1.427	4.800	.460	.875
1.200	.283	1.453	5.000	.425	.819
1.400	.361	1.465	5.200	.388	.762
1.600	.427	1.468	5.400	.349	.703
1.800	.481	1.461	5.600	.308	.643
2.000	.525	1.447	5.800	.264	.582
2.200	.559	1.427	6.000	.219	.520
2.400	.585	1.402	6.200	.173	.457
2.600	.603	1.372	6.400	.127	.394
2.800	.614	1.339	6.600	.083	.329
3.000	.619	1.303	6.800	.042	.263
3.200	.619	1.264	7.000	.006	.197
3.400	.613	1.224	7.134	.088	.088
3.600	.602	1.179			

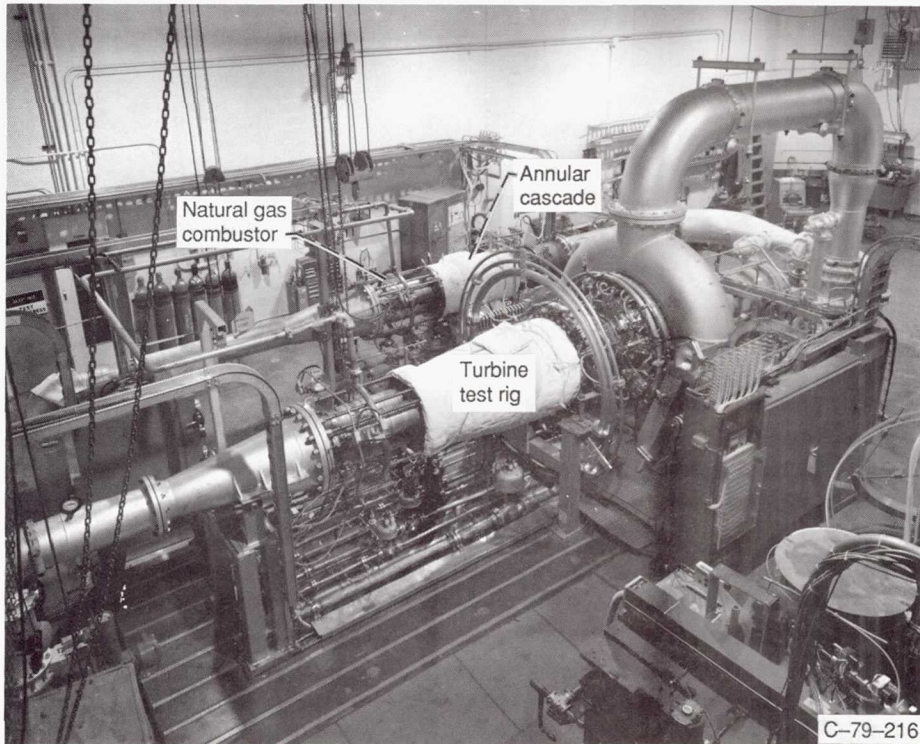


Figure 1.—Warm Core Turbine Facility.

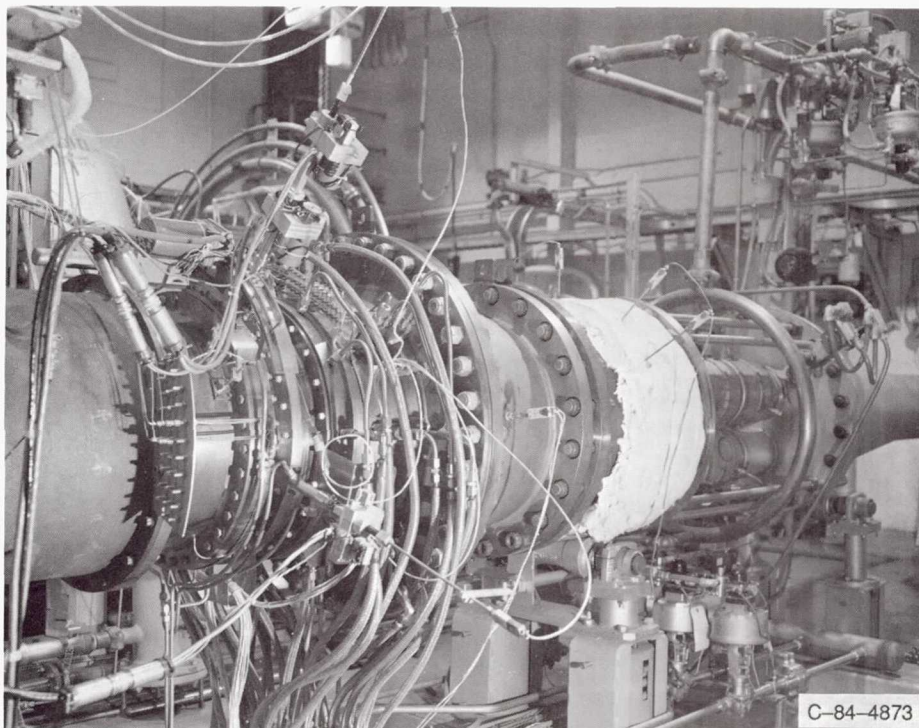


Figure 2.—Annular cascade test section.

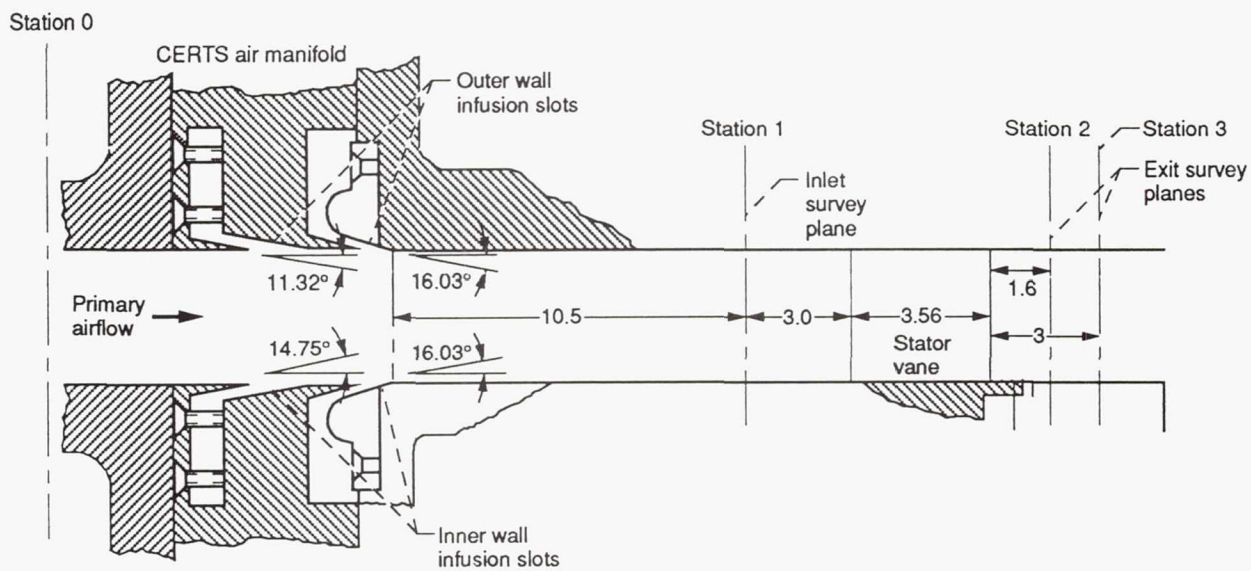


Figure 3.—Flowpath through turbine with CERTS inlet. (Linear dimensions are in centimeters.)

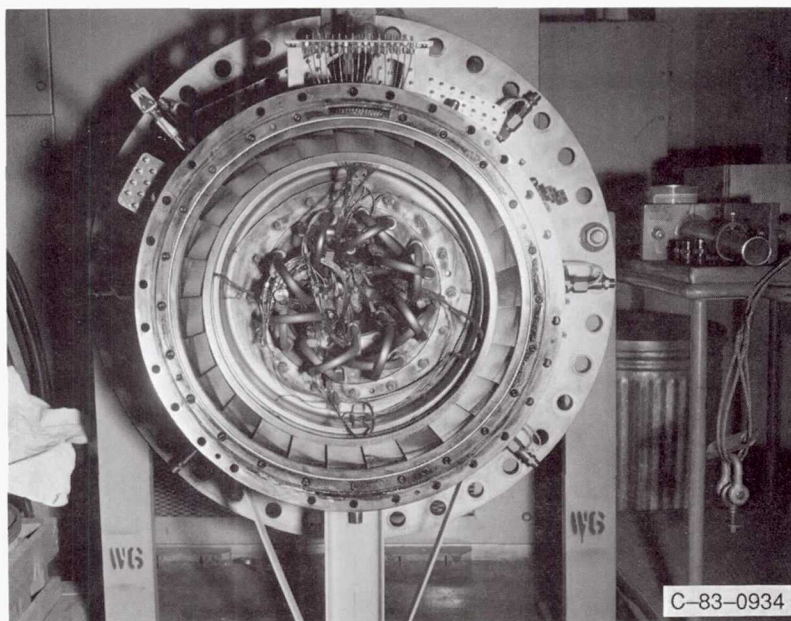


Figure 4.—Test stator.

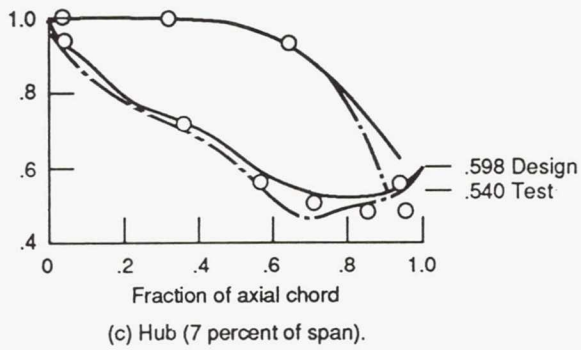
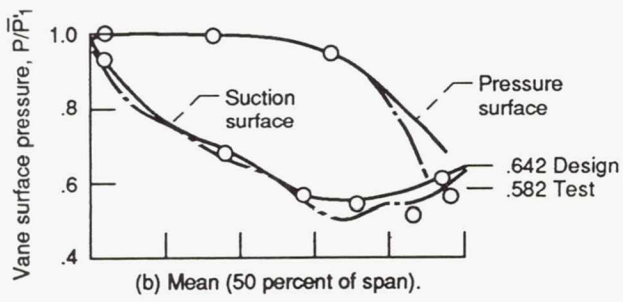
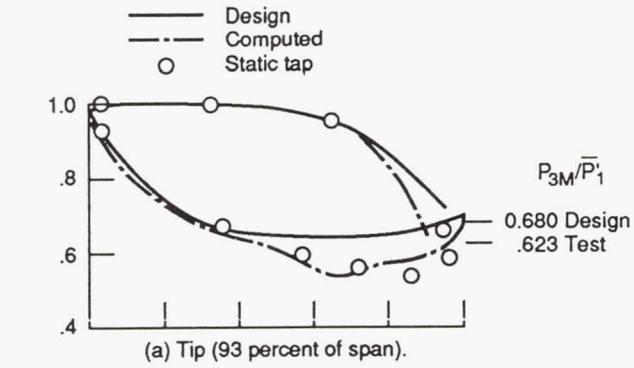


Figure 5.—Stator vane surface pressure distribution.

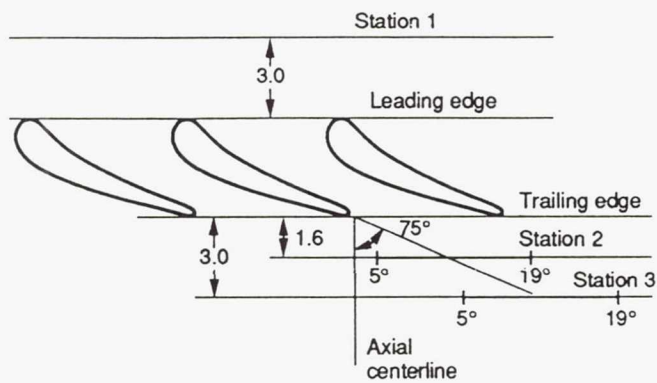


Figure 6.—Location of survey stations.

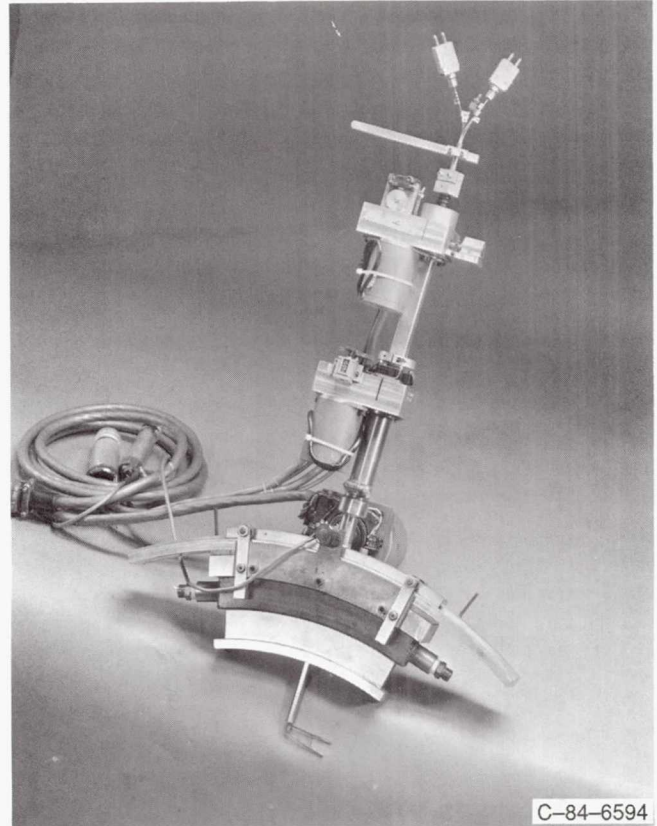


Figure 7.—Survey actuator and sting probe.

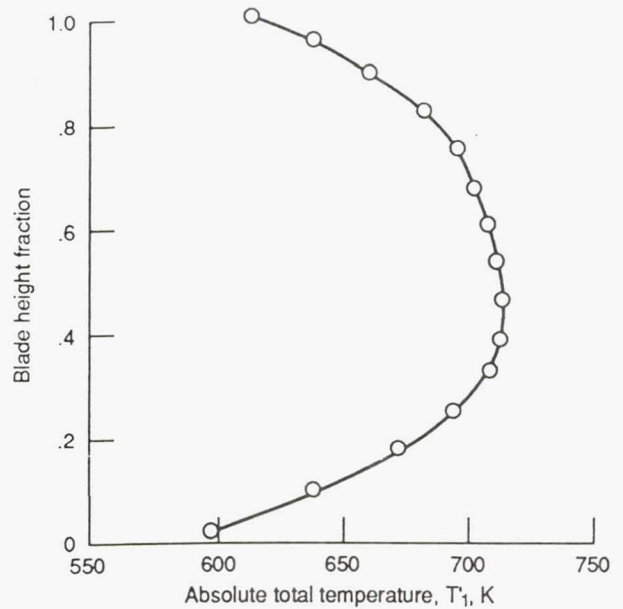


Figure 8.—Stator-inlet temperature profile.

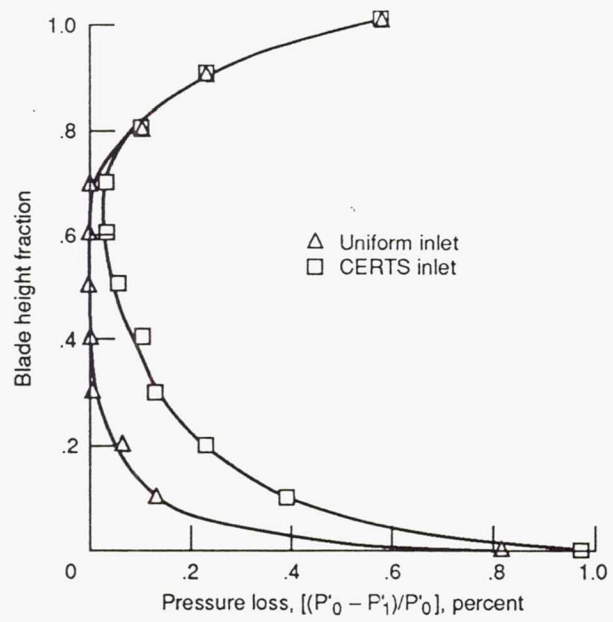
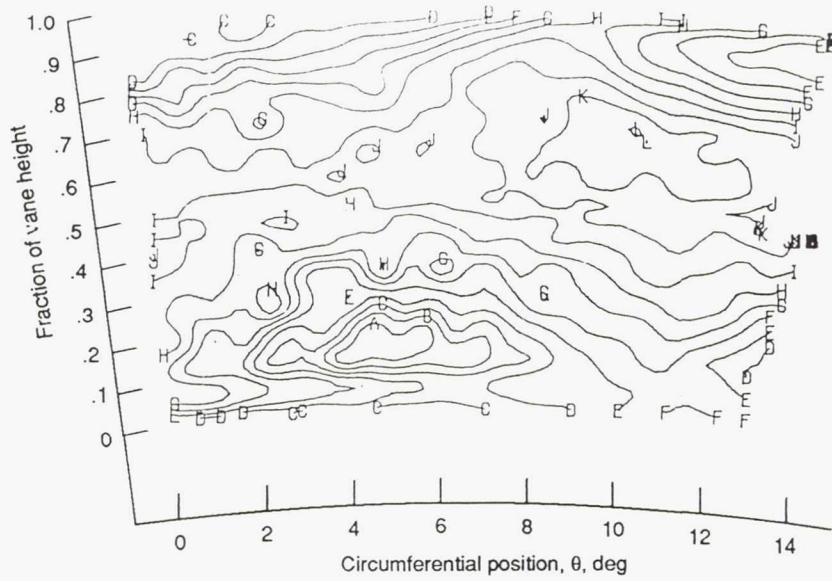
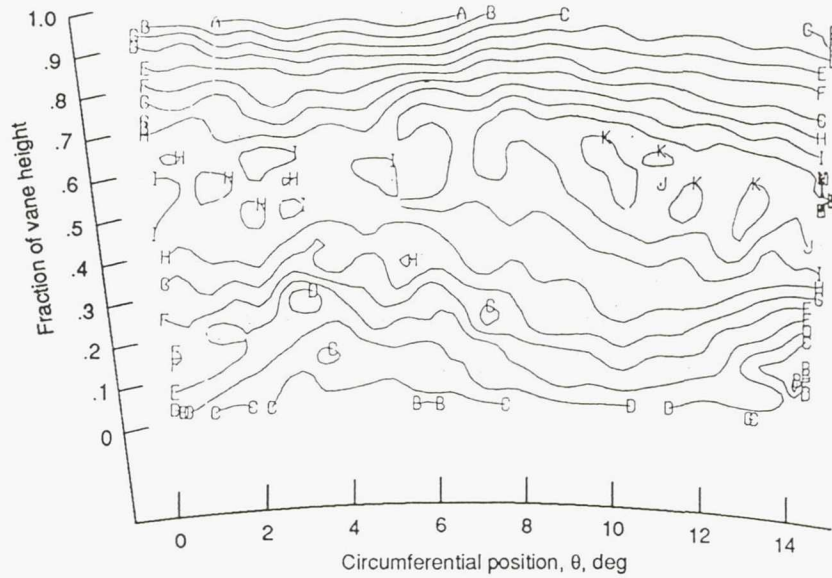


Figure 9.—Stator-inlet pressure loss.



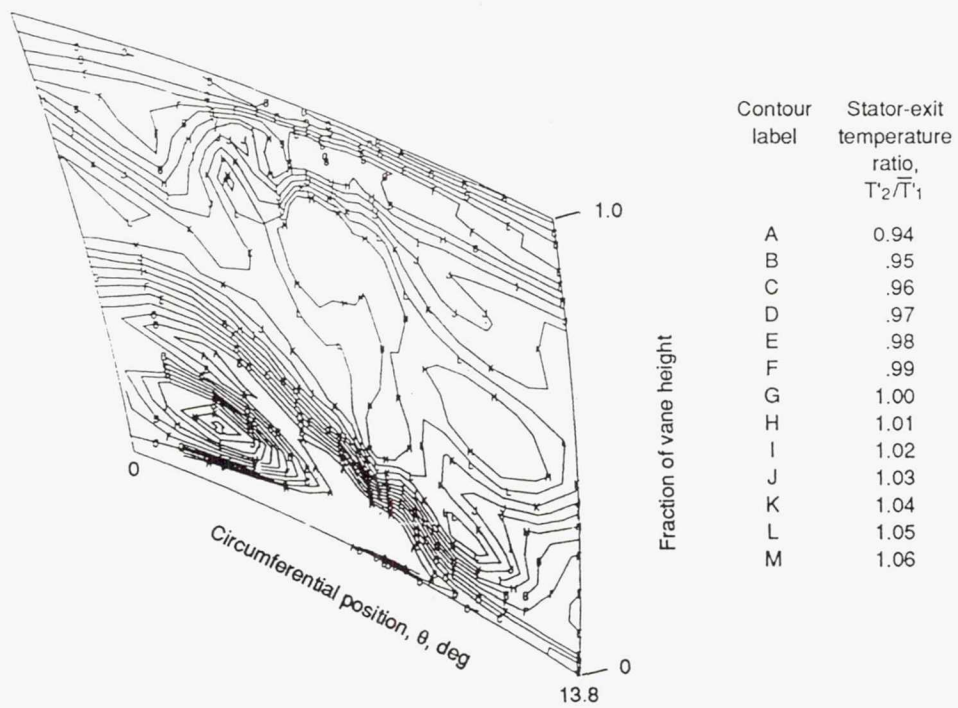
(a) At 1.6 cm.

Contour label	Stator-exit temperature ratio, T_2/T_1
A	0.94
B	.95
C	.96
D	.97
E	.98
F	.99
G	1.00
H	1.01
I	1.02
J	1.03
K	1.04
L	1.05
M	1.06

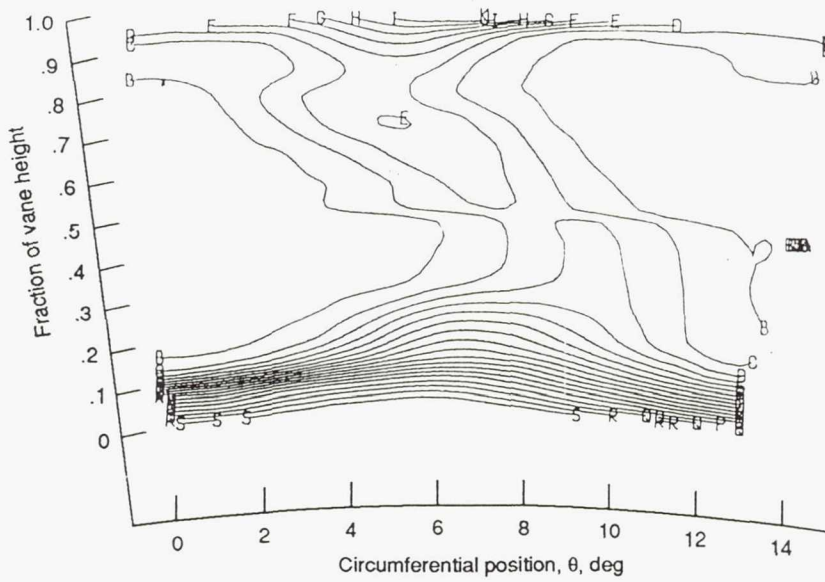


(b) At 3.0 cm.

Figure 10.—Stator-exit temperature ratio.

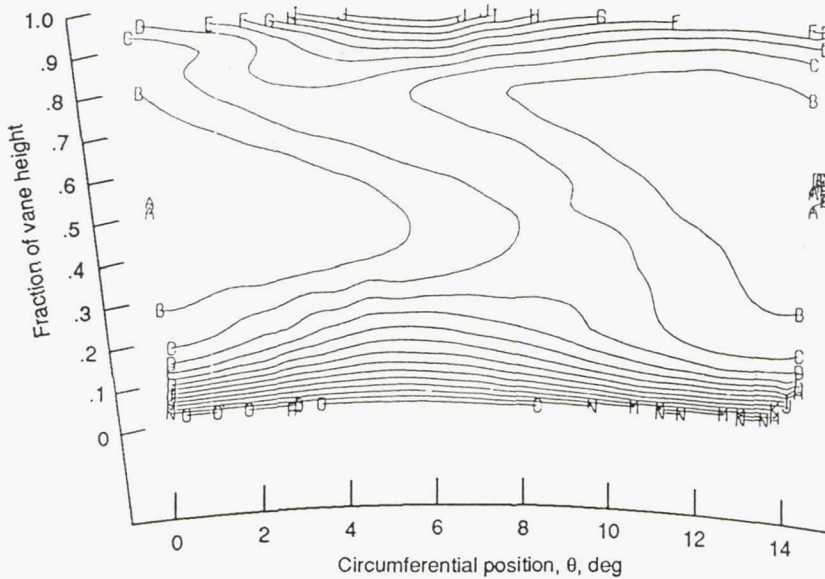


(c) Computed results.
Figure 10.—Concluded.



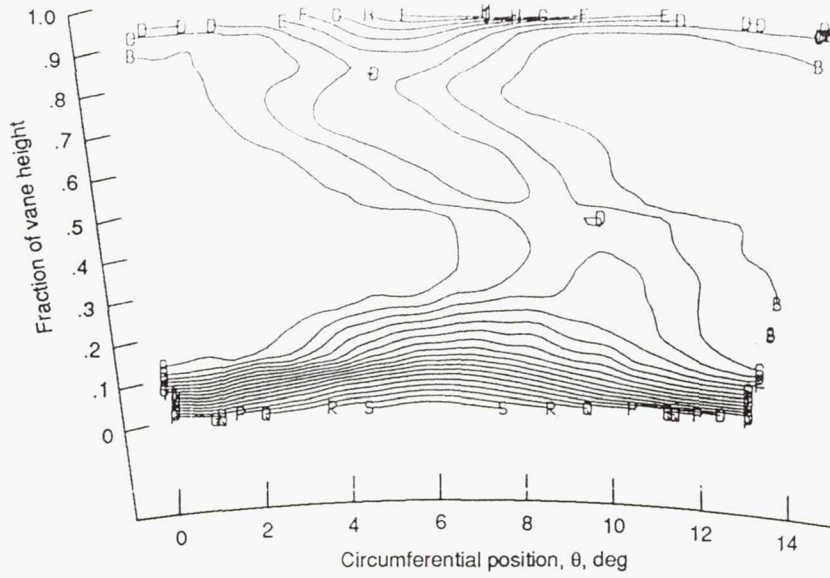
(a) At 1.6 cm with an inlet temperature profile.

Contour label	Stator-exit total pressure loss, $\frac{P'_1 - P'_2}{P'_1}$
A	0
B	.02
C	.04
D	.06
E	.08
F	.10
G	.12
H	.14
I	.16
J	.18
K	.20
L	.22
M	.24
N	.26
O	.28
P	.30
Q	.32
R	.34
S	.36



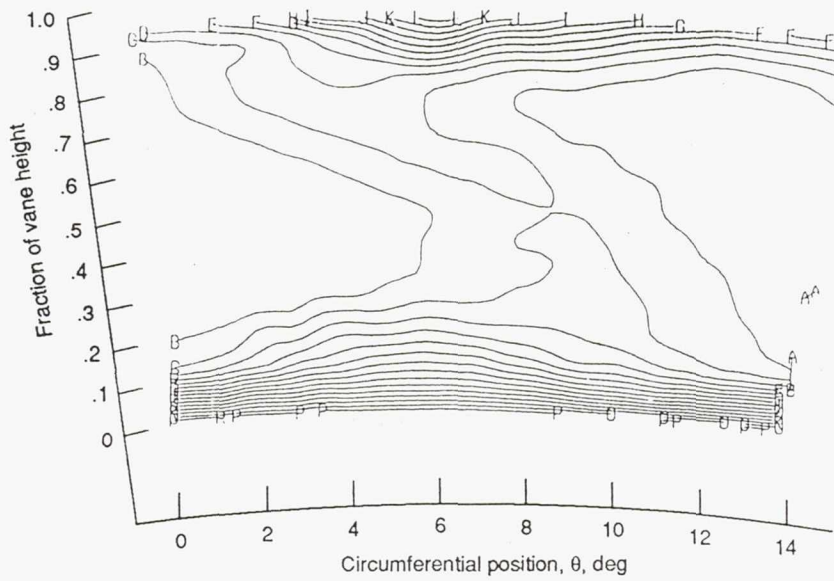
(b) At 3.0 cm with an inlet temperature profile.

Figure 11.—Stator-exit total pressure loss.



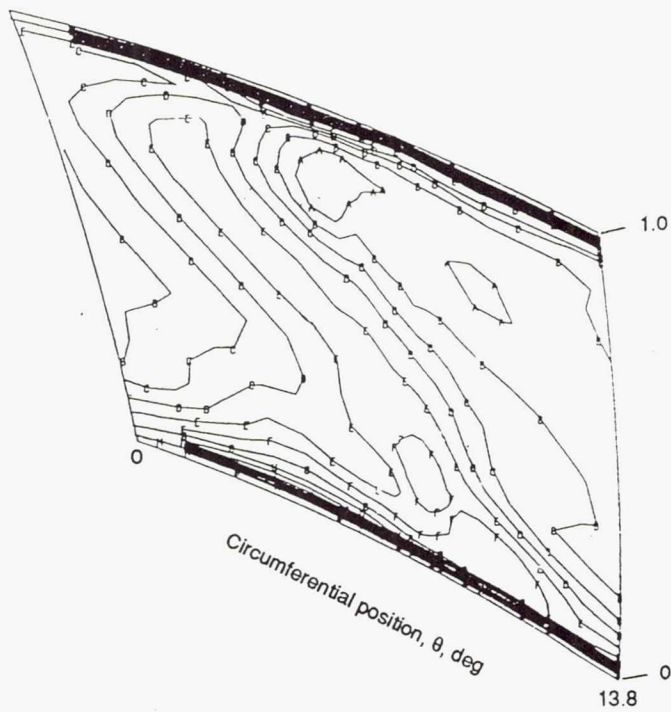
(c) At 1.6 cm with uniform inlet temperature.

Contour label	Stator-exit total pressure loss, $\frac{P'_1 - P'_2}{P'_1}$
A	0
B	.02
C	.04
D	.06
E	.08
F	.10
G	.12
H	.14
I	.16
J	.18
K	.20
L	.22
M	.24
N	.26
O	.28
P	.30
Q	.32
R	.34
S	.36



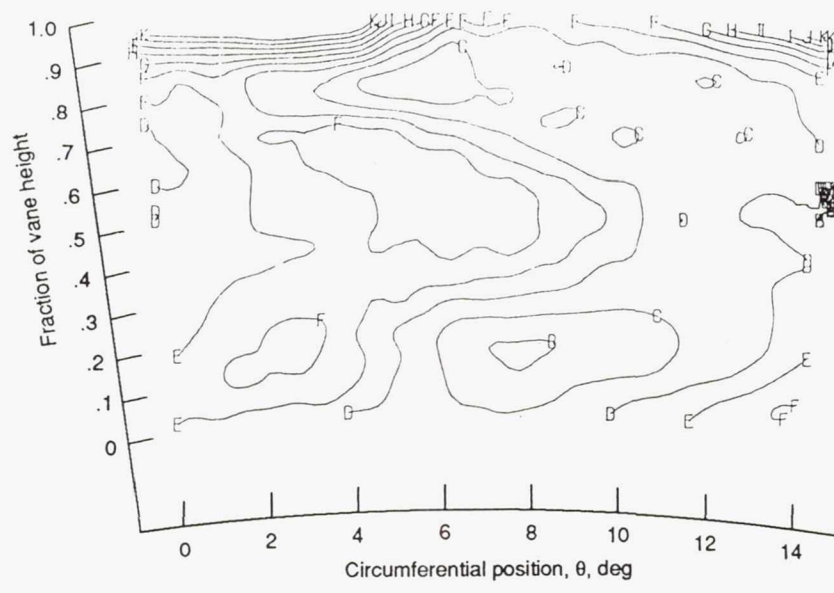
(d) At 3.0 cm with uniform inlet temperature.

Figure 11.—Continued.



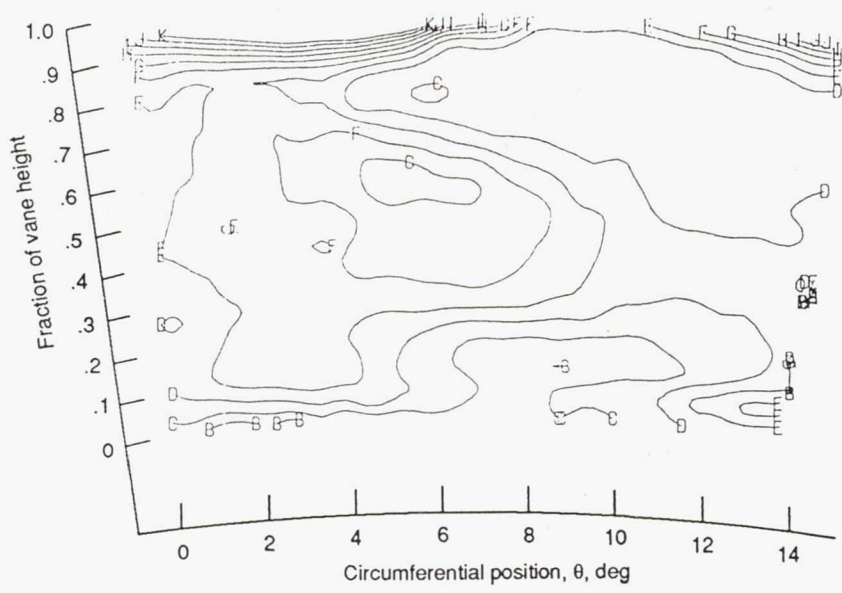
Contour label	Stator-exit total pressure loss, $\frac{P'_1 - P'_2}{P'_1}$
A	0
B	.02
C	.04
D	.06
E	.08
F	.10
G	.12
H	.14
I	.16
J	.18
K	.20
L	.22
M	.24
N	.26
O	.28
P	.30
Q	.32
R	.34
S	.36

(e) Computed results.
Figure 11.—Concluded.



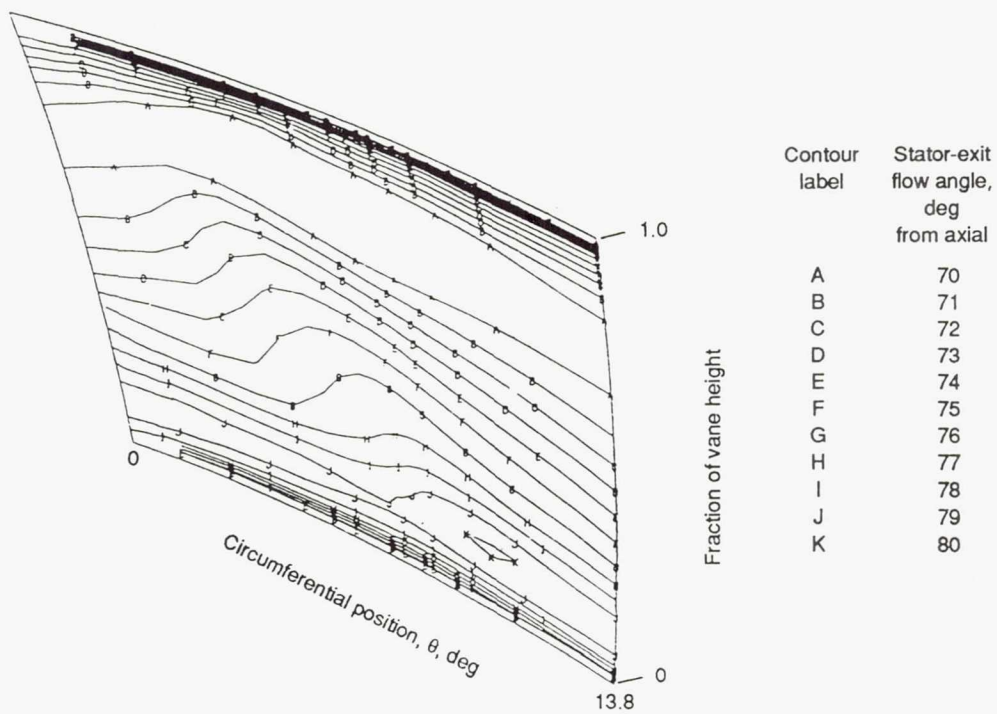
(a) At 3.0 cm with inlet temperature profile.

Contour label	Stator-exit flow angle, deg from axial
A	70
B	71
C	72
D	73
E	74
F	75
G	76
H	77
I	78
J	79
K	80

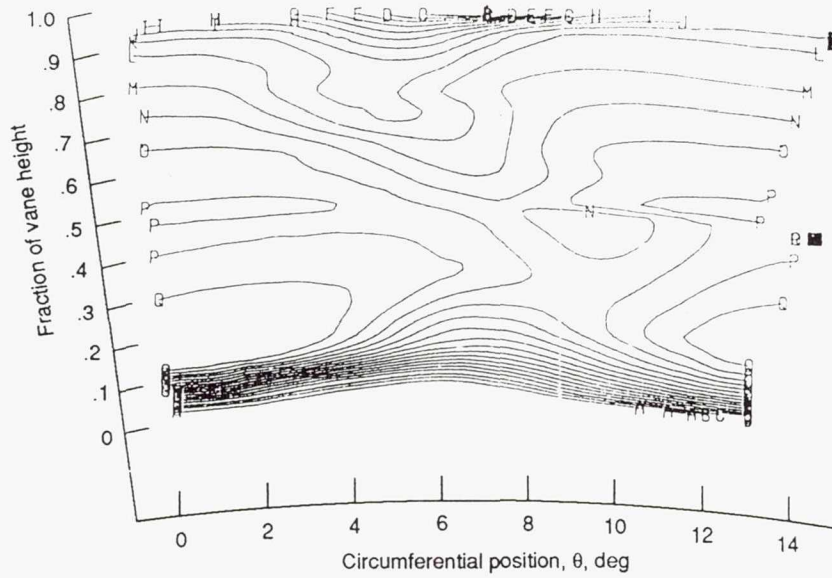


(b) At 3.0 cm with uniform inlet temperature.

Figure 12.—Stator-exit flow angle.

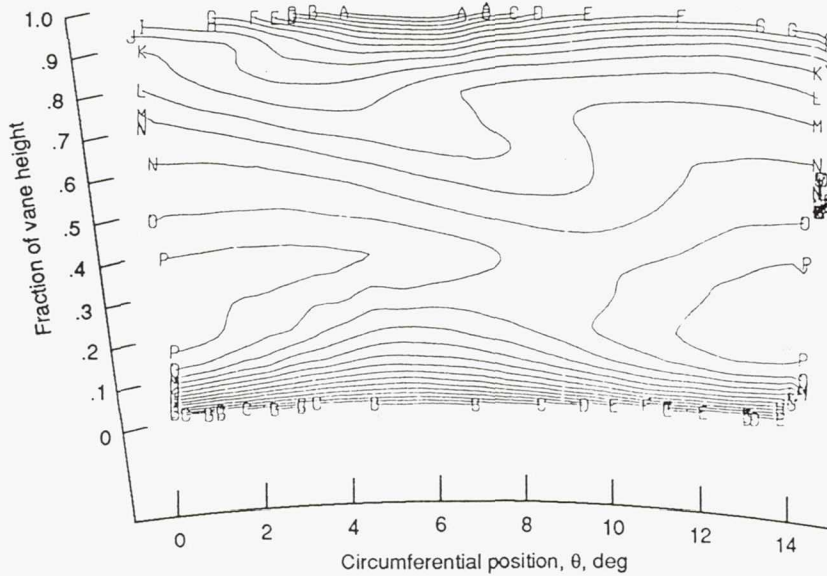


(c) Computed results.
 Figure 12.—Concluded.



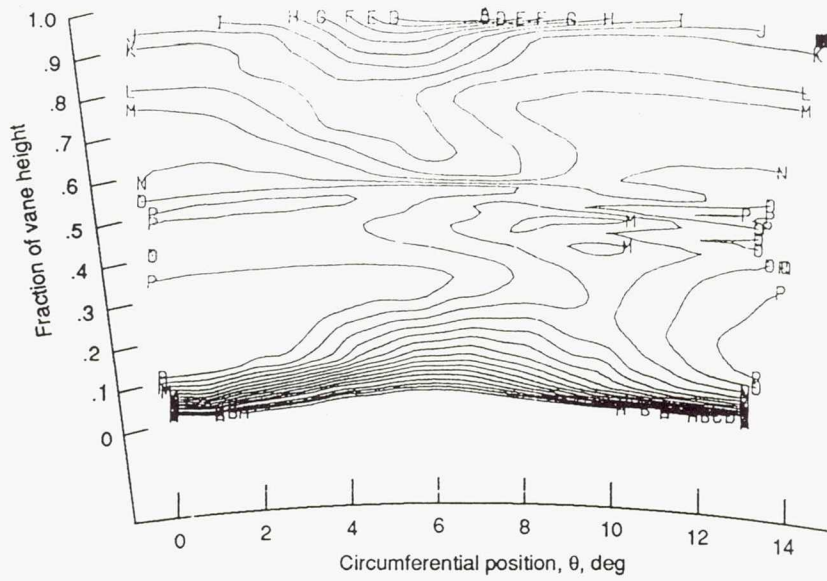
(a) At 1.6 cm with inlet temperature profile.

Contour label	Stator-exit Mach number
A	0.64
B	.66
C	.68
D	.70
E	.72
F	.74
G	.76
H	.78
I	.80
J	.82
K	.84
L	.86
M	.88
N	.90
O	.92
P	.94
Q	.96



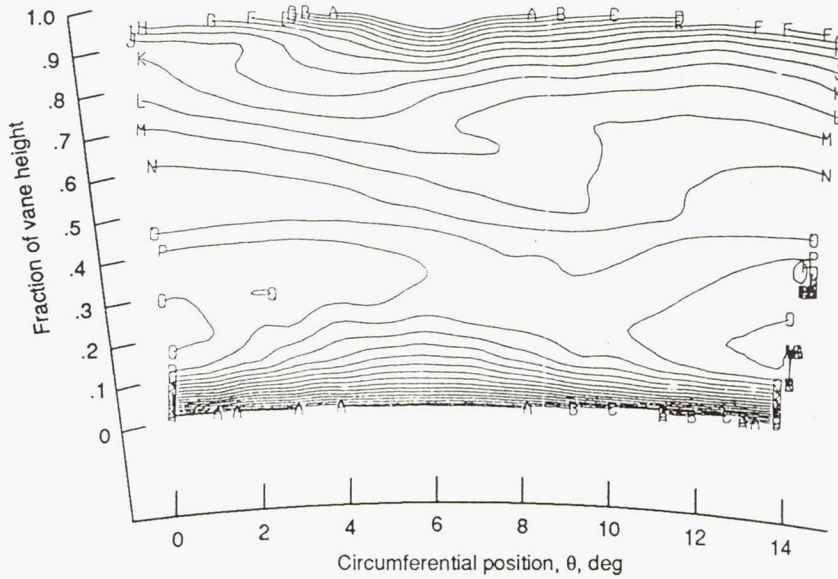
(b) At 3.0 cm with inlet temperature profile.

Figure 13.—Stator-exit Mach number.



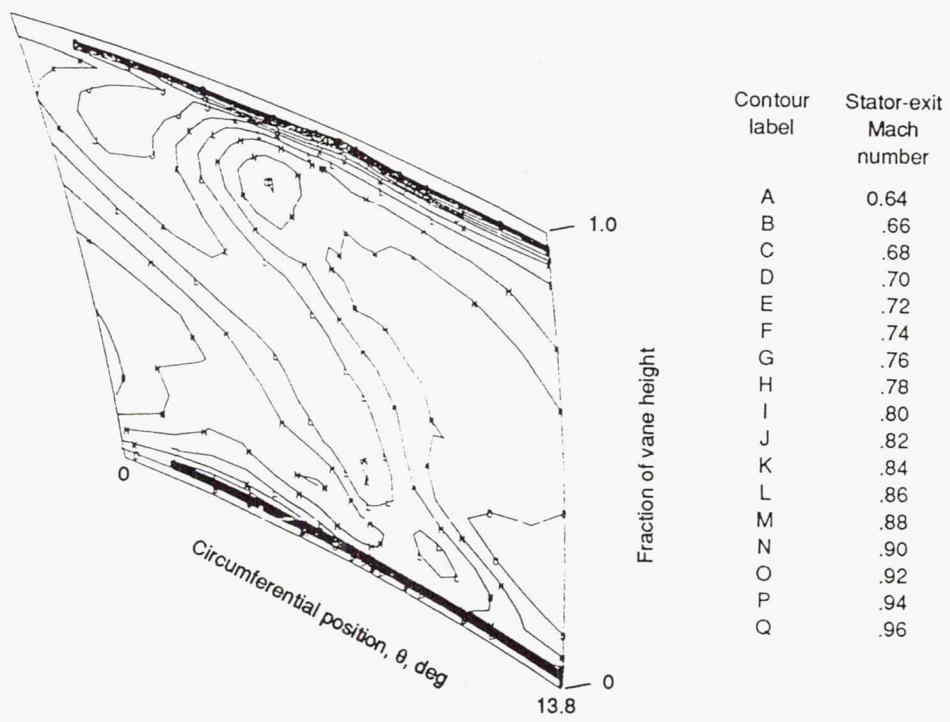
(c) At 1.6 cm with uniform inlet temperature.

Contour label	Stator-exit Mach number
A	0.64
B	.66
C	.68
D	.70
E	.72
F	.74
G	.76
H	.78
I	.80
J	.82
K	.84
L	.86
M	.88
N	.90
O	.92
P	.94
Q	.96

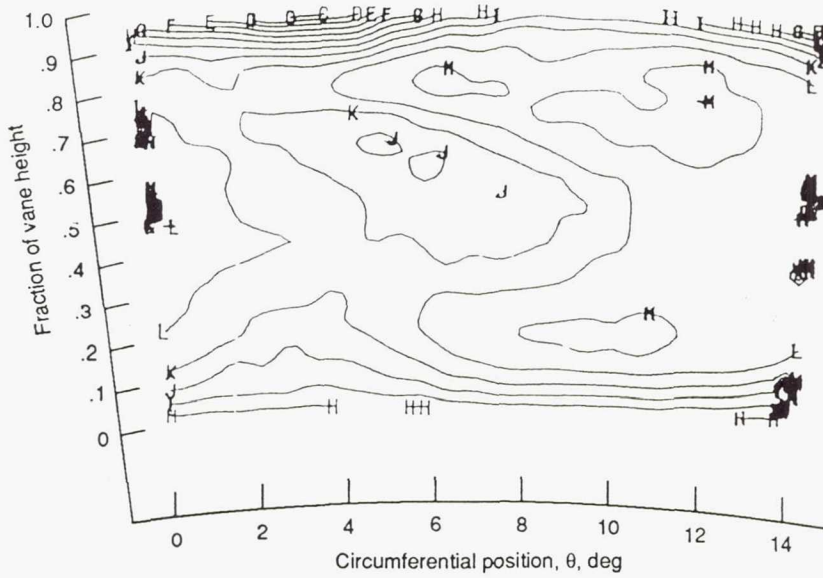


(d) At 3.0 cm with uniform inlet temperature.

Figure 13.—Continued.

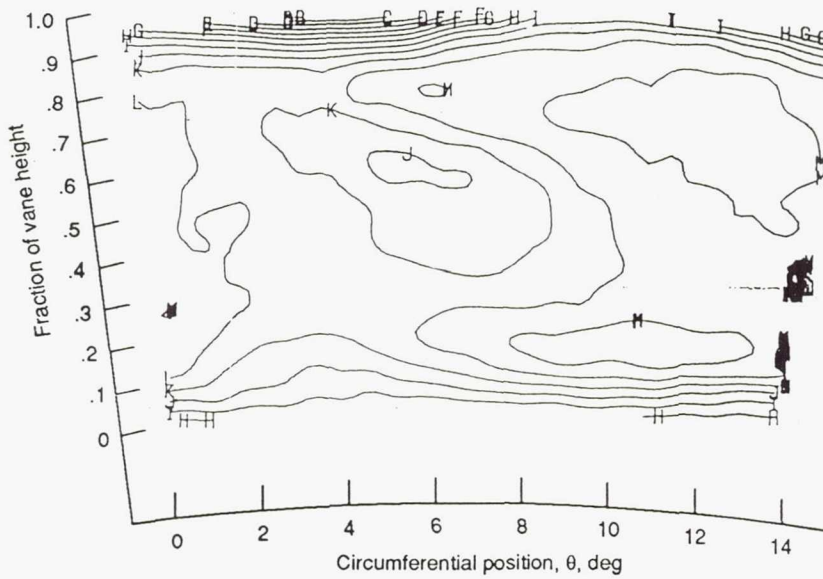


(e) Computed results.
 Figure 13.—Concluded.



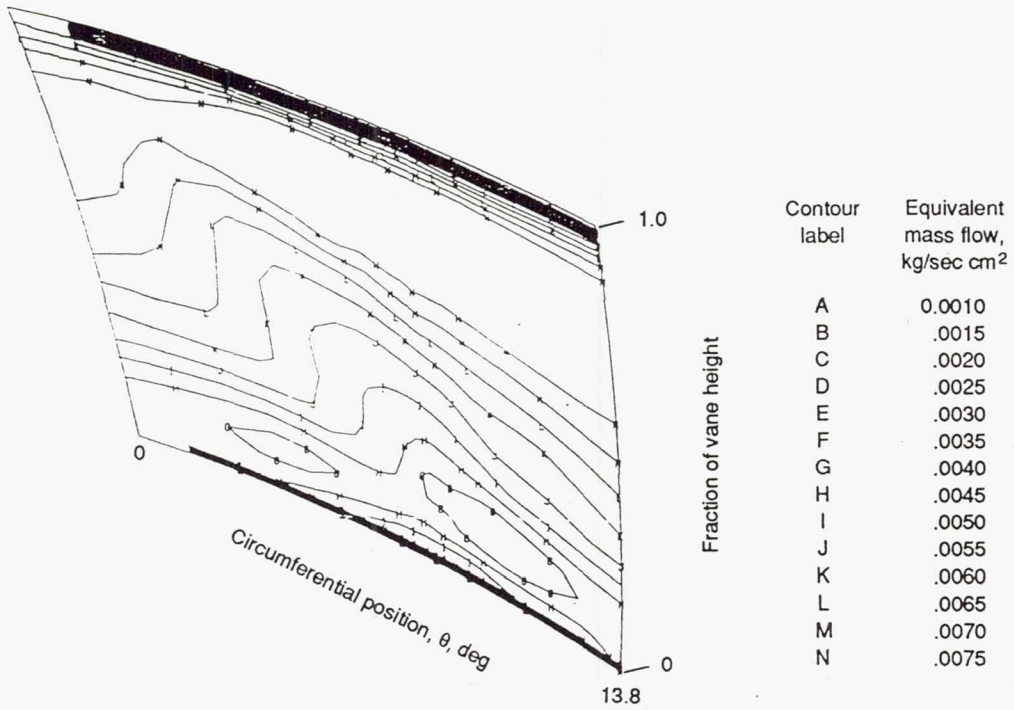
(a) At 3.0 cm with inlet temperature profile.

Contour label	Equivalent mass flow, kg/sec cm ²
A	0.0010
B	.0015
C	.0020
D	.0025
E	.0030
F	.0035
G	.0040
H	.0045
I	.0050
J	.0055
K	.0060
L	.0065
M	.0070
N	.0075



(b) At 3.0 cm with uniform inlet temperature.

Figure 14.—Stator-exit mass flow.



(c) Computed results.
Figure 14.—Concluded.

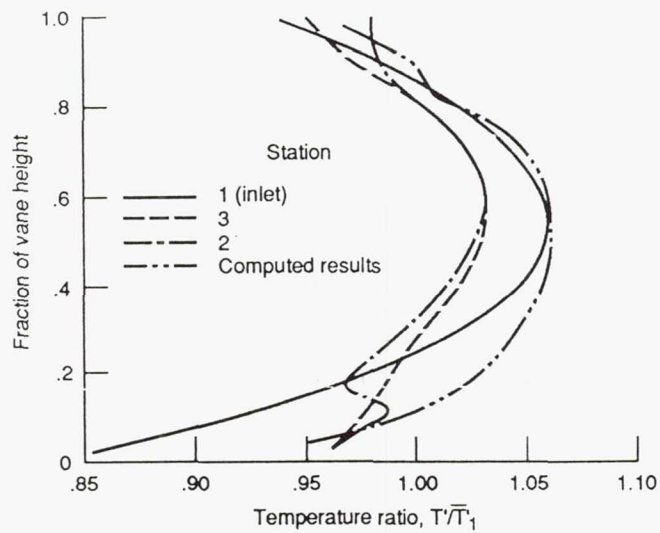


Figure 15.—Inlet and exit temperature profiles, 75° stator with CERTS inlet.

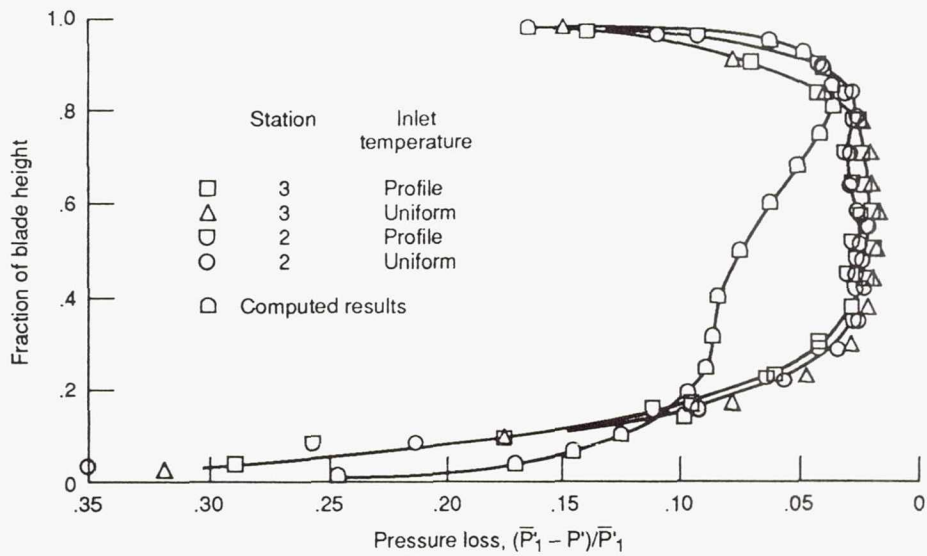


Figure 16.—Stator total pressure loss.

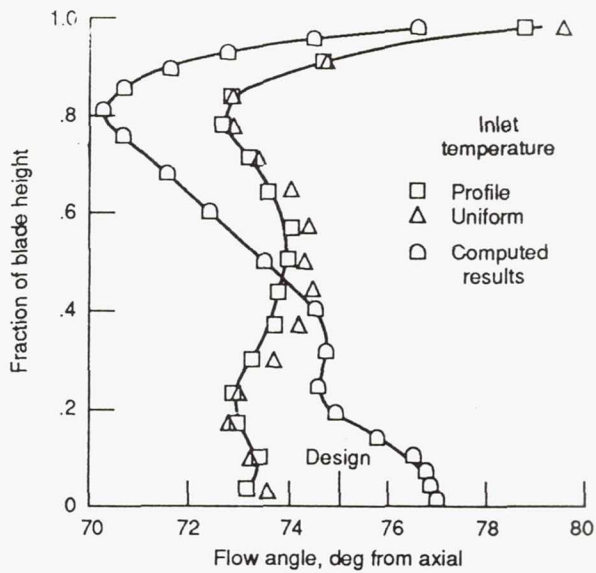


Figure 17.—Stator-exit flow angle.

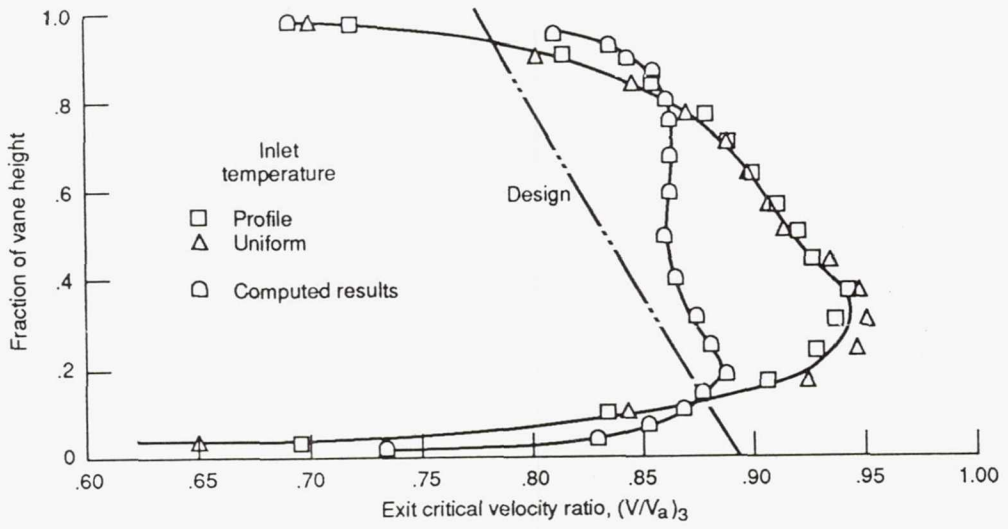


Figure 18.—Stator-exit velocity ratio.

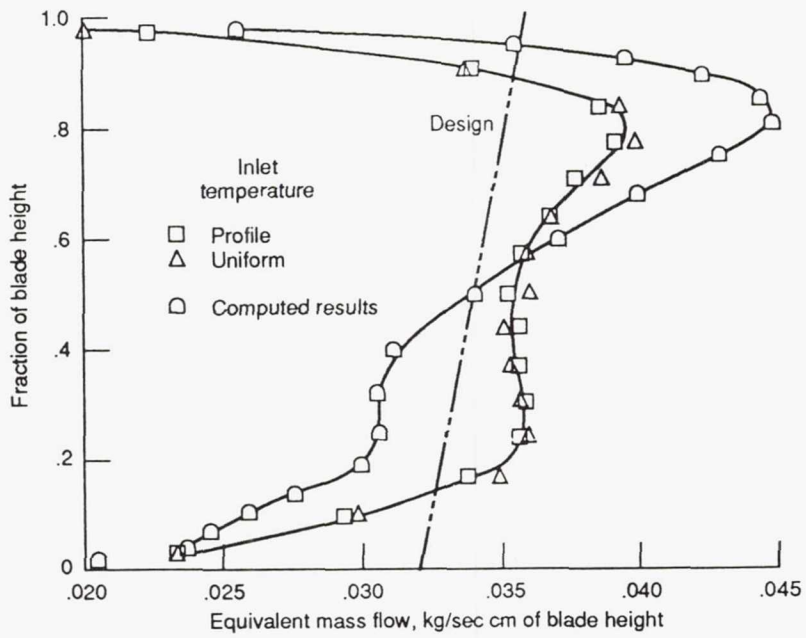


Figure 19.—Stator-exit mass flow.

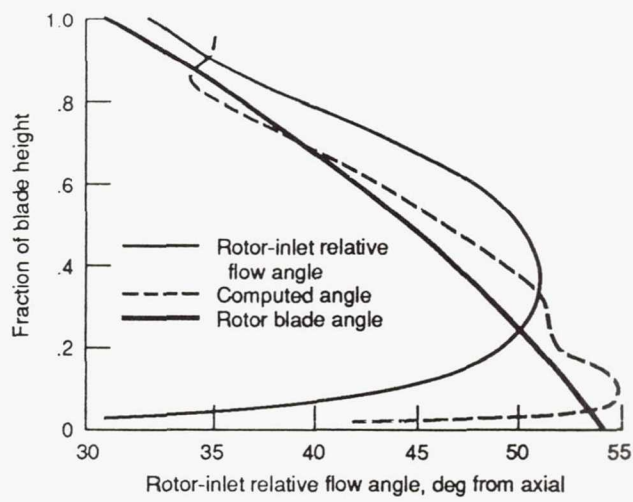


Figure 20.—Relative flow angle.

1. Report No. NASA TM-103738		2. Government Accession No.		3. Recipient's Catalog No.	
4. Title and Subtitle Performance of a High-Work, Low-Aspect-Ratio Turbine Stator Tested With a Realistic Inlet Radial Temperature Gradient				5. Report Date March 1991	
				6. Performing Organization Code	
7. Author(s) Roy G. Stabe and John R. Schwab				8. Performing Organization Report No. E-5975	
				10. Work Unit No. 505-62-3B	
9. Performing Organization Name and Address National Aeronautics and Space Administration Lewis Research Center Cleveland, Ohio 44135-3191				11. Contract or Grant No.	
				13. Type of Report and Period Covered Technical Memorandum	
12. Sponsoring Agency Name and Address National Aeronautics and Space Administration Washington, D.C. 20546-0001				14. Sponsoring Agency Code	
15. Supplementary Notes Responsible person, Roy G. Stabe, (216) 433-5700.					
16. Abstract A 0.767-scale model of a turbine stator designed for the core of a high-bypass-ratio aircraft engine was tested with uniform inlet conditions and with an inlet radial temperature profile simulating engine conditions. The principal measurements were radial and circumferential surveys of stator-exit total temperature, total pressure, and flow angle. The stator-exit flow field was also computed by using a three-dimensional Navier-Stokes solver. Other than temperature, there were no apparent differences in performance due to the inlet conditions. The computed results compared quite well with the experimental results.					
17. Key Words (Suggested by Author(s)) Turbines Tests Aerodynamics Navier-Stokes equation			18. Distribution Statement Unclassified - Unlimited Subject Category 07		
19. Security Classif. (of this report) Unclassified		20. Security Classif. (of this page) Unclassified		21. No. of pages 30	22. Price* A03